Printed in the Republic of Korea
ANALYTICAL SCIENCE & TECHNOLOGY
Vol. 32 No. 4, 121-130, 2019
https://doi.org/10.5806/AST.2019.32.4.121

Tandem laser-induced breakdown spectroscopy laser-ablation inductively-coupled plasma mass spectrometry analysis of high-purity alumina powder

Yonghoon Lee★ and Hyang Kim

Department of Chemistry, Mokpo National University, 1666 Yeongsan-ro, Jeonnam 58554, Korea

(Received April 29, 2019; Accepted August 1, 2019)

Abstract Alumina is one of the most important ceramic materials because of its useful physical and chemical properties. Recently, high-purity alumina has been used in various industrial fields. This leads to increasing demand for reliable elemental analysis of impurities in alumina samples. However, the chemical inertness of alumina makes the sample preparation for conventional elemental analysis a tremendously difficult task. Herein, we demonstrated the feasibility of laser ablation for effective sampling of alumina powder. Laser ablation performs sampling rapidly without any chemical reagents and also allows simultaneous optical emission spectroscopy and mass spectrometry analyses. For six alumina samples including certified reference materials and commercial products, laser-induced breakdown spectroscopy (LIBS) and laser-ablation inductively-coupled plasma mass spectrometry (LA-ICP-MS) analyses were performed simultaneously based on a common laser ablation sampling. LIBS was found to be useful to quantify alkali and alkaline earth metals with limits-of-detection (LODs) around 1 ppm. LA-ICP-MS could quantify transition metals such as Ti, Cu, Zn, and Zr with LODs in the range from a few tens to hundreds ppb.

Key words: Alumina, Laser ablation, LIBS, LA-ICP-MS

1. Introduction

Alumina (Al_2O_3) is used not only as a raw material for aluminum production but also as an anticorrosive material owing to its properties of wear resistance and minimal chemical reactivity. In addition, because it is also an excellent insulator against heat and electricity, alumina has been used as a source material in various sectors that need materials with such properties.[1,2] Recently, there is a growing demand for alumina powder with a high purity of ≥ 99.99 % and micrometer-level particle size in advanced industrial sectors, including display, energy material, automotive, and semiconductor sectors. In particular, sapphire ingots and wafers produced using high-purity alumina as a raw material are essential materials required for producing light-emitting diodes. Here, impurities in alumina may alter its optical properties. Accordingly, alumina impurity analysis is critical for quality control of the source material.

★ Corresponding author
Phone : +82-(0)61-450-2332 Fax : +82-(0)61-450-2339
E-mail : yhlee@mokpo.ac.kr

The most difficult process in impurity analysis of high-purity alumina could be viewed as sample pre-treatment. Alumina is physically very hard and chemically inert and thus makes the dissolution process of the solid-phase matrix complicated and time-consuming (10-20 h). Sample pre-treatment is typically conducted by dissolving alumina powder in an aqueous acid solution under a high-temperature and high-pressure condition.[3-6] Moreover, because the likelihood of the sample being exposed to contamination increases with the length and complexity of the sample preparation process, simplifying the sample pre-treatment process is very important for analyzing ultra-trace quantities of impurities in high-purity materials. Therefore, dry methods are more suitable for sampling materials, such as alumina, that are difficult to prepare in the solution phase, and the most commonly used dry sampling method for such purposes is the glow discharge method.[7-12] With dry sampling using glow discharge, the direct current (DC) discharge mode is typically used.[13] Therefore, when glow discharge is used, conductive samples can act as an electrode to allow effective sampling for mass spectrometry or optical emission spectroscopy; however, when analyzing nonconducting samples, such as alumina, separate electrode composed of expensive high-purity tantalum or indium must be used.

For dry sampling of nonconducting samples, laser ablation can be an effective alternative to glow discharge.[14] For laser ablation sampling, a femtosecond or nanosecond pulse laser is typically used. When the laser beam with a fluence of 10-100 GW/cm^2 is focused on the sample surface, the part of the sample where the laser energy is focused becomes atomized and ionized to produce plasma. This plasma has a lifestime of approximately several tens of microseconds and is extinguished as it emits light. By recording the optical emission spectrum, quantitative as well as qualitative analysis for the sample material can be performed. Moreover, the ablated particles can be directly sent to the mass spectrometer for elemental analysis. The elemental analysis method using the optical emission spectrum of laser-generated plasma is termed laser-induced breakdown spectroscopy (LIBS),[15,16] while the elemental analysis method using inductively-coupled plasma mass spectrometry on a solid sample atomized via laser ablation is termed laser-ablation inductively-coupled plasma mass spectrometry (LA-ICP-MS).[17] Accordingly, because both LIBS and LA-ICP-MS laser-induced plasma, they have the characteristic of being able to share the sampling process. Moreover, information regarding the elemental composition of the sample obtainable from these two analytical methods is mostly non-duplicative and complimentary. Generally, LIBS can analyze metallic elements with a limit of detection (LoD) of a few to several hundred ppm and nonmetallic elements with an LoD of several hundred ppm to several %.[18] The LoD performance of LIBS is even better for alkali and alkaline earth metals, sometimes reaching several hundred ppb. For relatively light elements, it is difficult to obtain reliable results from mass spectrometry using ICP-MS because of mass interference caused by molecules generated in the mass spectrometer and other isotopes with the same mass as the element being analyzed. However, this method has the advantage of offering excellent LoD performance for heavy elements. The LoD performance of LA-ICP-MS using laser ablation as the sampling method and ICP-MS as the detection method is generally superior to that of LIBS. For analysis of impurities contained in high-purity alumina samples, the LoD performance of LIBS is insufficient for most impurity elements as compared to that of LA-ICP-MS. However, LIBS may be an alternative in cases where reliable results for light alkali and alkaline earth metals, including Na, K, Ca, and Mg, cannot be obtained using ICP-MS because of the mass interference. It is widely known that ^{39}K, ^{40}Ca, and ^{24}Mg, the main isotopes of K, Ca, and Mg, respectively, are susceptible to mass interference by $^{38}Ar^{1}H^{+}$, $^{40}Ar^{+}$, and $^{12}C_2^{+}$ generated in the ICP-MS spectrometers using Ar plasma.[19-20] Moreover, ^{23}Na, the only isotope of Na, can be found as a background signal even when a sample has not been injected because of accumulated contamination inside the mass spectrometer.[21]

This paper reports that elemental analysis of light

metallic elements and heavy elements in high-purity alumina can be effectively performed using tandem LIBS/LA-ICP-MS using laser ablation. The feasibility of quantitative analysis was investigated using the intensity of the emission lines of the corresponding elements that appear in the LIBS spectra for light alkali and alkaline earth elements, such as Na, K, Ca, and Mg, and signal intensities of ^{49}Ti, ^{65}Cu, ^{66}Zn, and ^{90}Zr mass channels in ICP-MS for the heavier elements. As alumina samples, four certified reference materials (CRMs) and two commercial source materials were used. LIBS analysis results for Na, K, Ca, and Mg showed LoD values of 0.64, 2.4, 0.63, and 1.5 ppm, respectively. LA-ICP-MS analysis results for Ti, Cu, Zn, and Zr showed LoD values of 55, 58, 550, and 260 ppb, respectively.

2. Materials and Methods

2.1. Alumina samples

The samples used in the study consisted of three CRMs (R034, R035, and R035) prepared by the Ceramic Society of Japan, one CRM (8007-a) prepared by the National Metrology Institute of Japan, one commercial alumina product from Sumitomo Chemical (AKP-3000), and one commercial alumina product (HGH) from POS-HiAL. *Table* 1 shows the Na, K, Mg, Ca, Ti, Cu, Zn, and Zr concentrations chosen as the elements to be analyzed in this study for each sample. Among these, this concentrations of K, Ca, Ti, and Zn in the APK-3000 sample and Na, K, Mg, Ca, Ti, Cu, Zn, and Zr in the HGH sample were separately analyzed using an acid digestion method, as described in the following, prior to LIBS/LA-ICP-MS analysis. The sample (1.0 g) was placed in a 25-mL polytetrafluoroethylene (PTFE) container, which was then placed in a high-pressure container (Parr, Part No. 4746) for sample pre-treatment. After adding 15 mL of aqueous H_2SO_4 solution (Aldrich, 99.999 %) prepared to a volume ratio of 25 % to the container, the high-pressure container lid was tightly sealed and the container placed in an oven (at 230 °C) for 16 h. The sample pre-treated was then placed in a 100-mL volumetric flask and diluted until the H_2SO_4 concentration reached a volume ratio of 2 %. The liquid sample prepared in this manner was analyzed using inductively-coupled plasma atomic emission spectroscopy (ICP-AES) and ICP-MS. For the ICP-AES and ICP-MS analyses, Vision from Spectro and ELEMENT XR from Thermo Fisher Scientific were used, respectively. Standards from AccuStandard were used to obtain the concentration calibration curves for quantitative analysis.

Table 1. Certified concentrations of the elements contained in the samples. The unit for the tabulated values is ppm in terms of weight ratio

Element	R034	R035	R036	8007-a	AKP-3000	HGH
Na	13	1603	234	N.D.	0.4[a]	0.4[a]
K	17	4	2	N.D.	1.2[a]	0.8[a]
Mg	<0.6	7.8	3.6	2.8	1	0.3[a]
Ca	1	134	173	0.92	0.4[a]	0.6[a]
Ti	<1	17	19	0.26	0.3[a]	1.7[a]
Cu	<2	14	<2	0.92	1	0.2[a]
Zn	<2	10	6	N.D.	N.D.[a]	0.8[a]
Zr	<1	6.7	3	1.80	0.8[a]	0.9[a]

[a]From wet analysis using acid digestion method.

For the LIBS/LA-ICP-MS analysis using laser ablation sampling, alumina powder was pressurized to form pellets. Aluminum powder was placed in a pulverizer (Pulverisette 23, FRITSCH) together with aluminum oxide balls of a diameter of 10 mm and pulverized for 10 min of a rotational speed of 40 rpm. From the resulting powder, 5 g was taken and placed in a stainless-steel cup, to which a pressure of 1.3 kN/cm^2 was applied to form disc-shaped pellets with a diameter of 30 mm.

2.2. Experimental methods

A commercial LIBS instrument (J200 LIBS Instrument) from Applied Spectra, Inc. was used for laser ablation sampling. LIBS analysis could be performed in open air without a separate sample chamber; however, because tandem LIBS/LA-ICP-MS analysis was to be performed in this study, the alumina pellets were placed in a sample chamber, as shown in *Fig.* 1, and laser beam was focused on the sample surface with a 100 micrometer diameter spot.

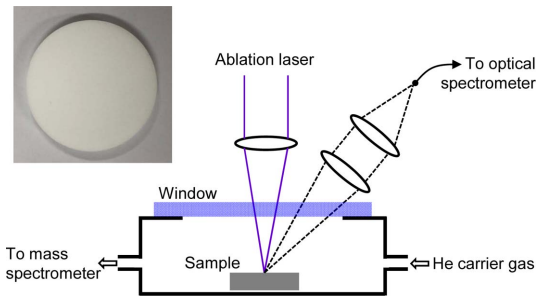

Fig. 1. A schematic diagram of the laser-ablation chamber. The inset is a picture of the alumina sample pellet.

A flash-lamp-pumped Q-switched Nd:YAG laser was used as the ablation laser. The wavelength, pulse width, and energy per pulse of this laser were set to 266 nm, 10 ns, and 15 mJ, respectively. The laser repetition rate was set to 10 Hz, and while the sample was being ablated, the stage holding the sample linearly moved at a speed of 0.2 mm/s. Accumulation of signals performed by linearly scanning a length of 2 mm on the sample surface under the aforementioned conditions led to a single measurement. The time required for the single measurement was 10 s. During this, 100 laser pulses were focused on the 2-mm scan line.

The light emitted from the plasma was received through two plano-convex lenses and introduced into a 6-channel spectrometer through an optical fiber. The spectrometer's wavelength coverage was 186-1050 nm, and the wavelength resolution was ~0.1 nm. The photodetector unit of the spectrometer was a charge-coupled device (CCD). From the laser Q-switching to the moment the CCD photodetector unit of the spectrometer began accumulating the light intensity, a difference of 500 ns in time was provided to avoid strong background continuum emission and broadening of atomic and ionic emission lines because of the high electron density of the initial plasma. The CCD was exposed to the light emitted from the plasma generated by each laser pulse for 1.05 ms. While recording the LIBS spectrum, particles ablated from the sample surface were sent to the mass spectrometer using helium gas to simultaneously record the signal intensity profiles at the mass-to-charge ratios m/z = 48(^{49}Ti), 63(^{65}Cu), 64(^{66}Zn), and 90(^{90}Zr). The flow rate of helium gas transporting the ablated particles from the sample chamber to the mass spectrometer (quadrupole mass spectrometer, Plasma Quant MS Elite, Analytik Jena) was 0.7 L/min.

3. Results and Discussion

3.1. LIBS

Fig. 2(a) shows the LIBS spectrum of the R035 sample in the wavelength range from 18 to 1050 nm. The strong emission lines observed in this spectrum were mostly because of Al and O. In addition to Al and O emission lines, Na I, K I, Ca II,

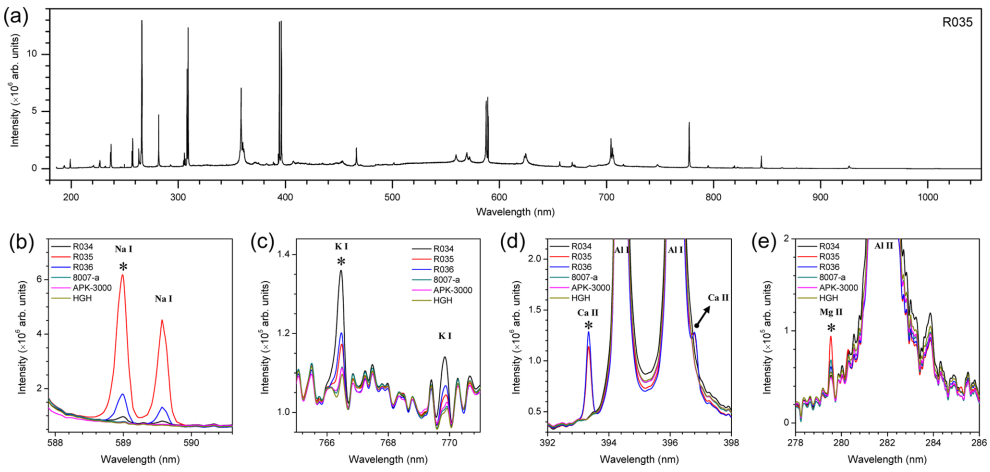

Fig. 2. (a) LIBS spectrum of the sample R035 in the wavelength region between 186 nm and 1050 nm and the expanded spectra around the strongest (b) Na I, (c) K I, (d) Ca II and (e) Mg II emission lines that are denoted by "*".

and Mg II emission lines were also observed near 589, 766, 393, and 280 nm, respectively. Each of these emission lines is marked in *Fig.* 2(b)-2(e), which show the spectra of the six alumina samples. Moreover, the emission line that showed the strongest intensity for each element is marked with an "*", and the intensity value of this emission line was used to obtain the concentration calibration curve. The emission line intensity value was calculated by integrating the area below the emission line after removing the baseline. *Fig.* 3 shows the concentration calibration curves of Na, K, Mg, and Ca obtained via LIBS analysis. For the concentrations of three CRMs prepared by the Ceramic Society of Japan (R034, R035, and R035) and one CRM prepared by the National Metrology Institute of Japan (8007-a), the certified values provided by the institutions were used. Whenever the upper limit value was provided, it was used to obtain the concentration calibration curve. For AKP-3000, the alumina product from Sumitomo Chemical, the impurity concentration data provided by the manufacturer were used, and for the impurity elements with no provided data, the values were obtained using the aforementioned acid digestion method. For HGH, the commercial alumina product from POS-HiAL, all elemental concentrations were obtained using the acid digestion method and were used to obtain the concentration calibration curves. The concentration calibration curves were derived by linear function fitting of the emission line intensities appearing in the LIBS spectrum for the certified concentration values or the analysis values using the acid digestion method. The R^2 values of linear fits for Na, K, Mg, and Ca were 0.9979, 0.8489, 0.9115, and 0.9978, respectively. Na and Ca showed the R^2 values close to 1, which indicated that the changes in emission line intensity appearing in the LIBS spectra according to the concentrations showed a greater

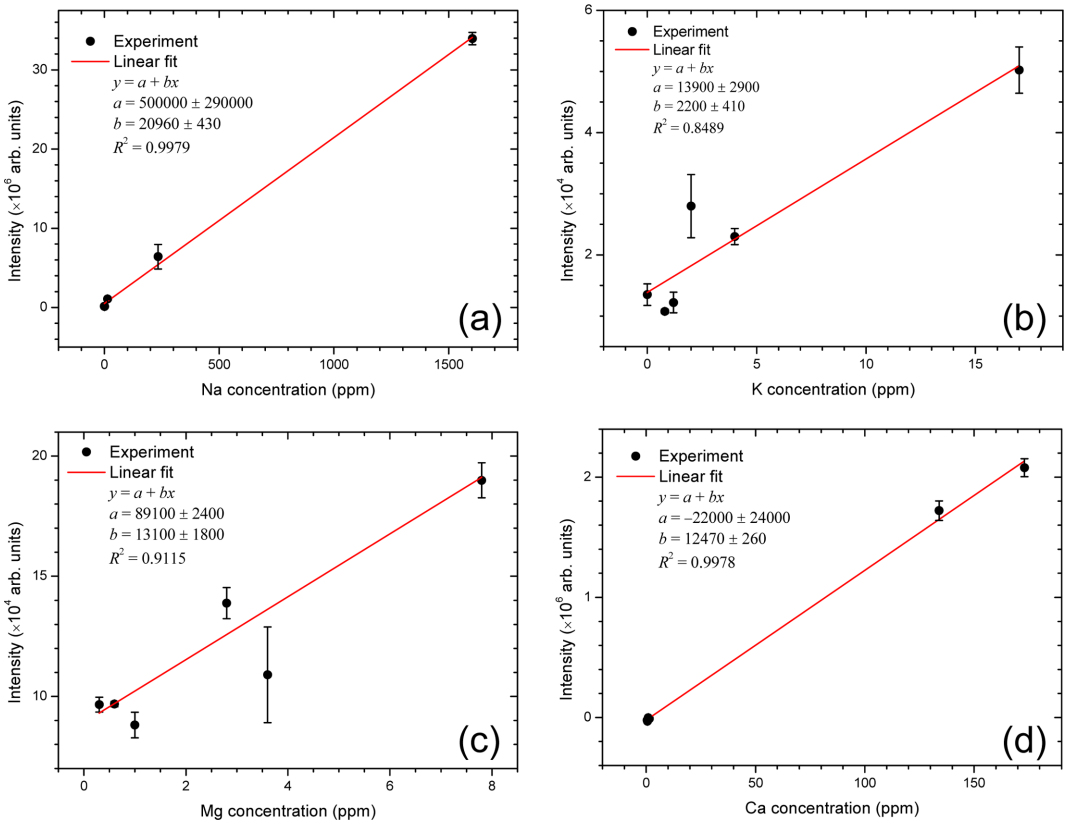

Fig. 3. Intensity-to-concentration calibration curves of (a) Na, (b) K, (c) Mg, and (d) Ca constructed on the basis of LIBS spectra.

linearity than those of K and Mg. The R^2 values for K and Mg showed a relatively large deviation from 1, which could be explained by the concentration range of the samples used for the concentration calibration curves being relatively narrower than those of Na and Ca and not because of poor accuracy in the elemental analysis. The sample concentration ranges for Na and Ca were 0-1650 and 0.4-173 ppm, respectively, whereas the ranges for K and Mg were relatively narrower at 0-17 and 0.3-7.8 ppm, respectively. The data used to obtain the concentration calibration curve for each element were used to calculate the root mean square error (RMSE) values for comparison. RMSE was calculated using Eq. (1) as follows:

$$\mathrm{RMSE} = \sqrt{\frac{\sum_{i=1}^{n}(\hat{y}_i - y_i)^2}{n}} \quad (1)$$

In Eq. (1), $\hat{y}_i$ is the certified concentration value or the concentration value obtained from the wet analysis; y_i is the predicted concentration value based on emission line intensity observed in the LIBS spectra and calibration curves; n is the number of LIBS spectra obtained from all samples; and i is the number assigned to each LIBS spectrum. Using Eq. (1), the RMSE values of Na, K, Mg, and Ca were calculated to be 44, 2.6, 1.3, and 4.3 ppm, respectively.

The large RMSE found in the Na concentration calibration curve could be explained by considering two factors: self-absorption and measurement precision. For quantitative analysis using LIBS, the sensitivity, in other words the concentration calibration curve slope, generally decreases with increasing concentration. Such a decreasing phenomenon in sensitivity according to concentration is known to occur because of self-absorption.[22] Self-absorption occurs because the temperature of the laser-induced plasma is spatially nonuniform. The outer part of the plasma that contacts the relatively cold air or ambient gas has a temperature that is relatively lower than that at the center. Generally, the light-receiving optical system in the LIBS spectrometer is aligned to focus on the plasma center where the signal is strongly measured. Under such conditions, light emitted from the plasma center passes through the outer part of plasma as it is directed toward the light-receiving optical system. There is a relatively large number of particles in the outer part of plasma, which are in the low-energy state because of the lower temperature, and as a result, the light emitted by the particles in the plasma center is reabsorbed. When self-absorption occurs in laser-induced plasma, its absorbance follows the Beer–Lambert law (Eq. (2)) as follows:

$$A = \log\frac{I_0}{I} = \varepsilon \cdot c \cdot l \quad (2)$$

In Eq. (2), A, I_0, I, e, c, and l represent the absorbance, incident light intensity, transmitted light intensity, extinction coefficient, concentration, and the distance for interaction between light and object, respectively. Therefore, having a broader concentration range for obtaining the concentration calibration curve makes it more difficult to obtain a linear calibration curve for the entire concentration range. The Beer–Lambert law indicates that the self-absorption intensity may vary according to not only the concentrations of the elements being analyzed but also the spectroscopic characteristics of the emission lines. In the liquid phase, e can represent the molar coefficient of extinction and c can represent the molar concentration. In plasma, these parameters can represent the Einstein coefficient for the light absorption process ($B_{\text{lower-upper}}$) and particle number density. In this case, self-absorption increases when $B_{\text{lower-upper}}$ is larger, where $B_{\text{lower-upper}}$ is proportional to the Einstein coefficient for the spontaneous emission process ($A_{\text{upper-lower}}$), as shown in Eq. (3). Therefore, even between emission lines from the same element, the emission line with a strong intensity shows more severe self-absorption phenomenon.

$$B_{\text{lower}-\text{upper}} = \frac{g_{\text{upper}}}{g_{\text{lower}}} \cdot \frac{c^3}{8\pi h \nu^3} \cdot A_{\text{upper}-\text{lower}} \quad (3)$$

In Eq. (3), g_{upper} and g_{lower} are the statistical weights (degrees of degeneracy) of the higher and lower energy states involving a certain transition, respectively, while c, h, and ν are the speed of light, Planck's

constant, and the frequency of absorbed or emitted light, respectively. Lastly, the characteristics of the lower energy state involved during the light emission process also affect the self-absorption intensity. The lower energy state of the emission line may be in the ground state or still in the excited state of which energy is lower than that of the initial excited state. Considering that the two energy states involved in self-absorption must be the same as the energy states involved in light emission, except that only the energy state during the initial and final stages changes, if the lower energy state of the emission line is still in an excited state and not the ground state, then the likelihood of self-absorption is significantly reduced because of the subsequent relaxation process. Therefore, self-absorption more severely appears when the lower energy state involved in the emission line is in the ground state. In the case of Na, the results can be explained by the fact that the calibration standards contain Na in the broader concentration range in comparison to K, Mg, and Ca; the lower energy state involved in the emission line was in the ground state; and changes in sensitivity due to the self-absorption effect readily appear when $A_{\text{upper-lower}}$ is large. *Table* 2 shows the spectroscopic constants of the emission lines used to obtain the concentration calibration curves of Na, K, Mg, and Ca. These constants were extracted from the National Institute of Standards and Technology Atomic Spectra Database.[23] The Na I emission line at 588.995 nm was the strongest among all Na I emission lines observed in the LIBS spectrum, which had the ground state as the lower energy state involved in the emission line at 588.995 nm. Therefore, because the Na concentration is 1603 ppm, which is much higher than those of other elements, there is a significant change in sensitivity between the low- and high-concentration regions. Accordingly, if a single linear function fitting is performed based on an assumption that there is no change in sensitivity over the entire concentration range, then the data obtained can significantly deviate from the fitting function, resulting in a large RMSE value. *Fig.* 4 shows the results of linear fitting with the concentration range divided into a low-concentration region (0-13 ppm) and a high-concentration region (13-1603 ppm). Compared to that of the low-concentration region, the slope of the calibration curve for the high concentration region is significantly smaller. Such a

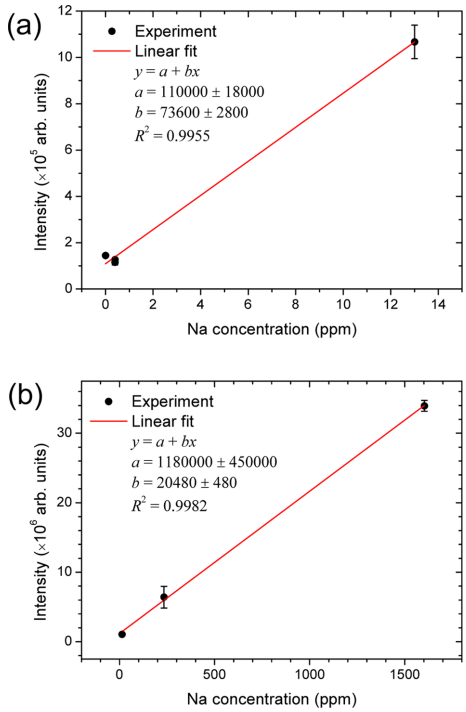

Fig. 4. (a) Intensity-to-concentration calibration curve of Na in the concentration range between 0 and 13 and (b) that between 13 and 1603 ppm.

Table 2. Spectroscopic parameters of Na I, K I, Mg II, and Ca II lines used for the calibration curves

Species	Wavelength (nm)	$A_{\text{upper-lower}}$ ($\times 10^7$ s^{-1})	E_{lower} (cm^{-1})	E_{upper} (cm^{-1})	g_{lower}	g_{upper}
Na I	588.995	6.16	0.00	16973.37	2	4
K I	766.490	3.78	0.00	13042.90	2	4
Mg II	279.553	26.0	0.00	35760.88	2	4
Ca II	393.366	14.7	0.00	25414.40	2	4

finding is highly consistent with the influence expected because of the self-absorption effect. The RMSE value calculated using the linear function obtained by fitting the low Na concentration region (0-13 ppm) was 1.0 ppm, which was similar to or actually lower than those of K, Mg, and Ca.

In the case of Na, K, Mg, and Ca, the relative standard deviations (RSDs), i.e., the ratio of the standard deviation of measured signal intensities to their average were 8, 10, 6, and 4 %, respectively. The RSD can be used as an indicator of analytical precision. Therefore, it can be viewed that the level of precision for the analysis conditions used on the alumina powder pellet samples in the present study was 4-10 % RSD. This precision performance showed an RSD of 2 % in the R035 sample with an Na concentration of 1603 ppm and an RSD of 10 % in the AKP-3000 sample with an Na concentration of 0.4 ppm. Accordingly, it was determined that the RSD is independent of the concentration at the given concentration range and the standard deviation (SD) increased at a rate similar to the increase in signal intensity or concentration. Under such conditions where RSD is independent of concentration, using samples with relatively high concentrations as the standards for obtaining the concentration calibration curves results in an increased RMSE, which is an indicator of accuracy. Therefore, the RMSE value that was especially large in Na could be explained by the influence of the RSD independent of concentration or signal intensity (the SD increased at a similar rate as that of the concentration or signal intensity) and self-absorption when the Na concentration range was much broader than that of the other elements in the samples used to obtain the concentration calibration curves.

The LoDs of the LIBS analysis for Na, K, Mg, and Ca were predicted under the given conditions. The LoDs were calculated using Eq. (4) as follows:

$$\mathrm{LOD} = \frac{3\sigma}{s} \tag{4}$$

In Eq. (4), s is the SD of the signal measured in the sample with low concentrations of elements being analyzed and *s* is the concentration calibration curve slope. The LoDs of Na, K, Mg, and Ca predicted using this method were 0.64, 2.4, 0.63, and 1.5 ppm, respectively.

3.2. LA-ICP-MS

Fig. 5 shows the mass signal intensity profiles of the R034, R035, R036, 8007-a, AKP-3000, and HGH alumina samples recorded at the *m*/*z* = 49 channel. The results show that the background signal intensity was approximately 10^3. These mass signal intensity profiles were simultaneously obtained with the LIBS spectrum. For simultaneous measurement using LIBS and LA-ICP-MS (single round), a linear scan was performed over a length of 2 mm above the sample surface while the sample stage rotated at a speed of 0.2 mm/s. Accordingly, the time required to record the mass signal was 10 s. Among the mass signal intensity profiles of the samples shown in *Fig.* 5, the sample with the highest Ti concentration was R036 with 19 ppm, the second highest was R035 with 17 ppm, and the third highest was HGH with 1.7 ppm. The other samples showed a Ti concentration less than 1 ppm. The measured mass signal intensity clearly showed correlations with the sample concentrations.

The mass signal intensity values used for the concentration calibration curves were obtained by removing the background signal from the mass signal intensity profile and integrating the area below the profile. *Fig.* 6 shows the concentration calibration

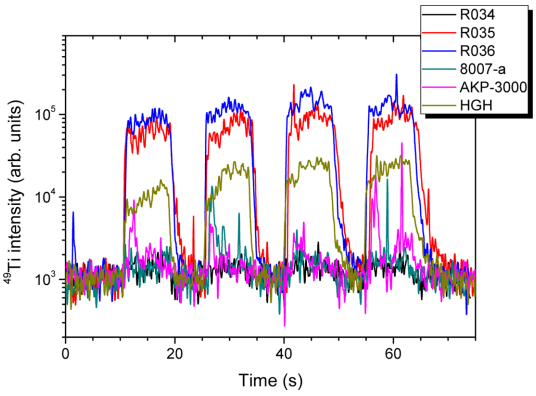

Fig. 5. Mass signal intensity profiles recorded at m/z = 49 (^{49}Ti) for the six alumina samples.

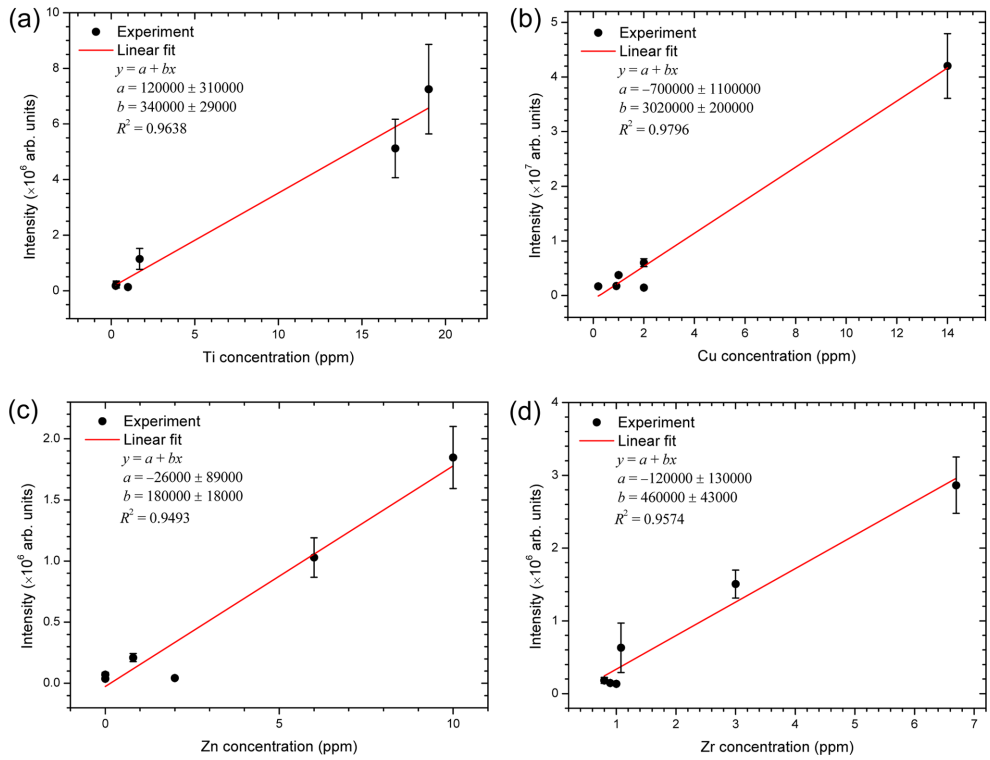

Fig. 6. Intensity-to-concentration calibration curves of (a) Ti, (b) Cu, (c) Zn, and (d) Zr constructed on the basis of LA-ICP-MS analysis.

curves obtained using the mass signal intensity values of ^{49}Ti, ^{65}Cu, ^{66}Zn, and ^{90}Zr and the concentrations of Ti, Cu, Zn, and Zr listed in *Table* 1. The concentration calibration curves are linear fits of the mass signal intensity values. After fitting, R^2 values were from 0.95 to 0.98. Similar to the LIBS analysis, Eq. (4) was used to predict the LoDs of Ti, Cu, Zn, and Zr, which are 55, 58, 550, and 260 ppb, respectively.

4. Conclusions

The present study investigated the feasibility of using a laser ablation sampling method for effective analysis of alumina powder impurities. Laser ablation is not only effective for sampling materials that are physically hard and chemically inert but it also has the advantage of LIBS analysis being simultaneously performed with mass spectrometry by sending the particles generated from the laser-ablated samples. This study performed tandem LIBS/LA-ICP-MS analysis on six samples including alumina CRMs and commercial products. LIBS analysis results showed that, along with the Al and O emission lines, which are the main elements comprising the matrix, those of Na, K, Mg, and Ca were observed. The intensities of these emission lines were then used to obtain the concentration calibration curves. In the case of Na, the RMSE, which could be viewed as an indicator of analytical accuracy, was larger than that of all the other elements, and accordingly, the reasons for such a difference were discussed. The LIBS analysis results for Na, K, Ca, and Mg showed a LoD of 0.64, 2.4, 0.63, and 1.5 ppm, respectively. Along with the LIBS spectrum, mass signal intensity profiles for the m/z = 49, 65, 66, and 90 channels were simultaneously obtained via LA-ICP-MS analysis. The results were then used to obtain the concentration calibration curves of Ti, Cu, Zn, and Zr. Under the given LA-ICP-MS conditions, the LoDs of Ti, Cu, Zn, and Zr were 55, 58, 550, and 260 ppb, respectively.

Based on the findings in the present study, it was determined that by using laser ablation sampling, a LIBS analysis with a LoD performance of approximately 1 ppm is possible for alkali and alkaline earth metals while simultaneous analysis at a level of several tens to several hundred ppb for transition elements is possible. The LIBS spectrum presented in this study was recorded using a linear CCD photodetector. Therefore, it is believed that by using an intensified CCD, a photodetector with superior LoD performance, and increasing the number of laser pulses used for laser ablation to perform a single round of measurements to a number higher than 100, the performance of the tandem LIBS/LA-ICP-MS analysis could be even further enhanced.

Acknowledgements

This research was supported by a research grant from Mokpo National University in 2017.

References

1. P. Atkins and L. Jones, 'Chemical Principles The Quest for Insight', W. H. Freeman and Company, New York, 2008.
2. Y. L. Wu, J. Hong, D. Peterson, J. Zhou, T. S. Cho, and D. N. Ruzic, *Surf. Coat. Technol.*, **237**, 369-378 (2013).
3. G. Molnár, J. Borossay, Z. B. Varga, M. Ballók, and A. Bartha, *Mikrochim. Acta*, **134**, 193-197 (2000).
4. H. Matusiewicz, *Mikrochim. Acta*, **111**, 71-82 (1993).
5. M. T. Larrea, I. Gómez-pinilla, and A. C. Fariñas, *J. Anal. At. Spectrom.*, **12**, 1323-1332 (1997).
6. H.A. Foner, *Anal. Chem.*, **56**, 856-859 (1984).
7. S. Jung, S. Kim, and J. Hinrichs, *Spectrochim. Acta B*, **122**, 45-51 (2016).
8. N. Jakubowski, T. Prohaska, L. Rottmann, and F. Vanhaecke, *J. Anal. At. Spectrom.*, **26**, 693-726 (2011).
9. N. Jakubowski, T. Prohaska, F. Vanhaecke, P. H. Roos, and T. Lindemann, *J. Anal. At. Spectrom.*, **26**, 727-757 (2011).
10. W. Schelles, S. D. Gendt, V. Muller, and R. V. Grieken, *Appl. Spectrosc.*, **49**, 939-944 (1995).
11. V. Hoffmann, M. Kasik, P. K. Robinson, and C. Venzago, *Anal. Bioanal. Chem.*, **381**, 173-188 (2005).
12. M. Kasik, C. Venzago, and R. Dorka, *J. Anal. At. Spectrom.*, **18**, 603-611 (2003).
13. J. C. Woo, N. Jakubowski, and D. Stuewer, *J. Anal. At. Spectrom.*, **8**, 881-889 (1993).
14. R. E. Russo, X. Mao, J. J. Gonzalez, V. Zorba, and J. Yoo, *Anal. Chem.*, **85**, 6162-6177 (2013).
15. F. J. Fortes, J. Moros, P. Lucena, L. M. Cabalín, and J. J. Laserna, *Anal. Chem.*, **85**, 640-669 (2013).
16. D. W. Hahn and N. Omenetto, *Appl. Spectrosc.*, **66**, 347-419 (2012).
17. N. L. LaHaye, M. C. Phillips, A. M. Duffin, G. C. Eiden, and S. S. Harilal, *J. Anal. At. Spectrom.*, **31**, 515-522 (2016).
18. A. W. Miziolek, V. Palleschi, and I. Schechter, 'Laser-Induced Breakdown Spectroscopy (LIBS) Fundamentals and Applications', Cambridge University Press, Cambridge, 2006.
19. S. H. Tan, and G. Horlick, *Appl. Spectrosc.,* **40**, 445-460 (1986).
20. E. Albalat, P. Telouk, V. Balter, T. Fujii, V. P. Bondanese, M.-L. Plissonnier, V. Vlaeminck-Guillem, J. Baccheta, N. Thiam, P. Miossec, F. Zoulim, A. Puisieux, and F. Albarede, *J. Anal. At. Spectrom.*, **31**, 1002-1001 (2016).
21. S.-H. Nam, H. Chung, J.-J. Kim, and Y.-I. Lee, *Bull. Korean Chem. Soc.*, **29**, 2237-2240 (2008).
22. J. P. Singh and S. N. Thakur, 'Laser-Induced Breakdown Spectroscopy', Elsevier Science, Amsterdam, 2007.
23. NIST Atomic Spectra Database, https://www.nist.gov/pml/atomic-spectra-database.

Authors' Positions

Yonghoon Lee : Professor
Hyang Kim : Graduate Student